v. 3, n. 35, 2023

Journal of
Engineering
Research

SURFACE POTENTIAL MAPPING OF Na-β-ALUMINA AND Na-β-ALUMINA /TZ3Y WITH KELVIN PROBE FORCE MICROSCOPY

Samuel da Silveira Martins
University of São Paulo, São Carlos School of Engineering, SP

Vera Lúcia Arantes
University of São Paulo, São Carlos School of Engineering, SP

Abstract: Solid-state sodium beta-alumina (Na-β-alumina) batteries are promising candidates for next-generation energy storage devices. New methods to characterize electrochemical reactions that occur during battery operation are necessary in order to understand the fundamental principles of batteries performance and improve their performance. In this work, the use of 3%mol yttria stabilized zirconia (TZ3Y) and Na-β-alumina with of Kelvin probe atomic force microscopy (KPFM) to obtain images of the internal electrical potential distribution of the electrolytes. TZ3Y is one of the most commonly used oxygen ions conductors, by incorporating low valence cations as rare earth, it is possible to zirconia stabilizes the cubic and tetragonal phases of ZrO_2 as well as improve its mechanical and electrical propertie.It was possible to visualize the electrical potential distribution throughtout the solid electrolyte. The observed results of the electrolyte show the behavior of the phases and the state of homogeneity present on the surface. The method improves the evaluation of fundamental aspects of the electrolyte to improve device performance, including the evaluation of the distribution of electrical potential depleted regions and the visualization of the topology present on the surfaces.

INTRODUCTION

Development of sodium based batteries had a great interest major on what during the 1970s and 1980s, and are currently marketed for stationary applications. In anticipation to a predicted shortage of lithium and consequent increase in price, sodium batteries have been investigated again after almost 50 years of their invention. Sodium is abundant earth's crust, present low cost and has a redox potential very close to that of lithium.

Sodium-based batteries can operate at high temperatures and have high energy density, high charge/discharge efficiency and long life cycle. They are based on a beta-alumina electrolyte membrane (Na-β-alumina) that acts as a sodium ion conductor between the electrodes, significantly affecting battery performance [1-3]. The β-alumina phase presents has the chemical formula $Na_2O.11Al_2O_3$ [4] while the β´´-alumina phase $Na_2O.5Al_2O_3$ [5]. According to the $Na_2O.Al_2O_3$ phase diagram proposed by Fally et al. [6], β/β´´ structures coexist in the region corresponding to the $Na_2O.nAl_2O_3$ formula, resulting in a mixture of β-alumina/β´´-alumina phases [7].

Na-β-alumina is generally manufactured via conventional solid-state reaction. This method involves calcination of a mixture of Na_2CO_3, α-Al_2O_3 and Li_2CO_3 or MgO at 1200 to 1250°C followed by sintering at 1600°C [8-10]. However, this method has several disadvantages [10,11] Na_2O evaporates from the due to the high sintering temperature and the abnormal growth of the grain during sintering weakens the material.

TZ3Y is one of the most commonly used oxygen ions conductors [12,13]. Pure zirconia (ZrO_2) has a monoclinic structure up to a temperature of around 1173°C, in which it changes to the tetragonal structure. At high temperatures, zirconia adopts a fluorite-type cubic structure. Yttria is the most commonly used dopant to stabilize the cubic phase of zirconia.

By incorporating low valence cations as rare earth, it is possible to zirconia stabilizes the cubic and tetragonal phases of ZrO_2. Due to the evolution of the ceramic oxide purification processes and also due to its characteristics, yttrium oxide (yttria) has improvemed its mechanical and electrical propertie[14,15]. The addition of substitutional cation (Y^{3+}) with lower valence than zirconium ion (Zr^{4+}) can induce the generation of oxygen vacancies

for charge compensation. The replacement of Zr^{4+} by Y^{3+} causes a negative charge in the network for each mol of yttrium incorporated in the zirconia network [3].

TZ3Y provides a pathway for the diffusion of the oxygen ion as well as the yttrium ion in its structure. The ionic conductivity occurs owring to transport throug oxygen vacancies, it is transported between these voids [16,17]. The sodium ions are transported between the spinel blocks of Na-β-alumina [3,10]. The addition of TZ3Y to Na-β-alumina can improve its fracture and without decrease of its electrical properties for use of a solid electrolyte. In addition to extending the battery life using these materials, increase of the charge current density can shorten the charging time [18-20].

This makes it possible to consider them to be a modern, efficient energy source for various applications – from stationary power and heat supply for the industrial, residential, and transport (light and heavy vehicles, aircraft, ships, auxiliary power units) sectors, to portable power supply systems [21]. In this context, one of the most important obstacles is their high operating temperatures, which leads to a significant reduction in the range of possible structural materials, reduces service life and increases the cost of manufacturing for the device as a whole [21-25]. The solution to this problem involves the search for, and development of, alternative, in particular electrolyte, materials characterised by high oxygen-ion or proton conductivity [26-30].

Na-β-alumina batteries has taken much of attention due to the demands for high densification and increased ionic conduction capacity. Much can be improved in its processing using characterization techniques such as atomic force microscopy and Kelvin probe atomic force microscopy (AFM-KPFM). However, solid Na-β-alumina electrolytes have some disadvantages such as low energy densities caused by high ionic resistivity at the interfaces between the active material and the electrode. For the fundamental understanding of the origin of the interfacial resistivity, new techniques are demanded to measure the distribution of the electrical potential and/or ion concentration of cells.

Kelvin probe atomic force microscopy (KPFM) has been widely used to characterize the electrical potential distribution of various electronic and ionic devices. In the study of electronic ceramic devices, electrical potential distributions were measured under applied voltage conditions to obtain information about the electron transport properties. On the other hand, the studies were restricted to measurements only on the surface of the electrolyte, that is, not in the interface regions [21,22] (image 1). For this reason, the information obtained to consider the fundamental properties of the electrolyte, such as high ionic resistivity at the interfaces and the distribution of electrical potential, were very limited.

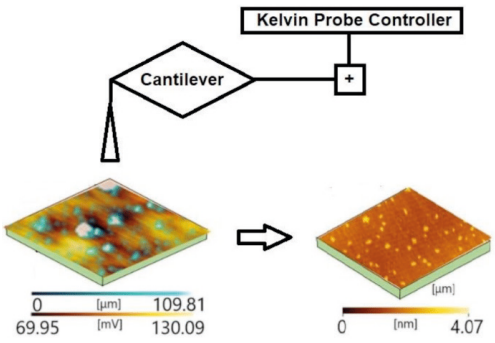

Figure 1: Schematic illustration for the KPFM model, presents the recorded contact potential. Brighter region indicates higher recorded contact potential difference. A lower represents a higher work function.

In this work, development of ceramics based on Na-β-alumina and ceramic composite Na-β-alumina/TZ3Y (zirconia partially stabilized with 3% yttria) were carried out. We were able to visualize the distribution

of electrical potential in the interface regions between the Na-β- alumina ceramic and the Na-β- alumina/TZ3Y ceramic composite in a composite electrolyte, using the atomic force microscopy characterization technique Kelvin (AFM/KPFM). The method reveal to be efficient to characterize fundamental aspects of this electrolyte to improve the performance of the device, including the evaluation of the distribution of impoverished regions of electrical potential and the visualization of the topology present on the surfaces.

EXPERIMENTAL PROCEDURE

MATERIALS AND METHODS

For this work, pure α-Al_2O_3 (99.9% - Alcoa, USA) and ZrO2 were used was used as starting material and with the addition 3%mol yttria stabilized zirconia (TZ3Y - Tosoh, Japan) were dried and sprayed with an area specific surface area of 16 ± 3m²/g and crystallite size of about 50nm.

The powders were mixed according to the weight percentagence of the oxides, in isopropyl alcohol using a high energy mill (Frizstch, model Pulverisette 4), in zirconia flasks with a 3:1 ball ratio, using 20 mm diameter zirconia spheres as media grinding at 400 rpm for 8 h. The suspensions were dried and calcined. After, they were formed by uniaxial pressing to form cylindrical tablets with a diameter of 6 mm and a height of 10 mm. Then they were pressed in an isostatic press (AIP CP 360) for 2 minutes at 200 MPa. The relative green densities were maintained at as (55 ± 2)% of the theoretical density.

The nomenclature of the different powder mixtures directly reflects their composition. 90β-10Z, for example, refers to the powder mixture with 90% by volume of Na-β-alumina and 10% by volume of TZ3Y (Table1).

Samples	%wt.Na-β-alumina	%wt.TZ3Y
100 β	100	-
90β10Z	90	10
80β20Z	80	20
70β30Z	70	30

Table 1: Nomenclature of the sodium beta-alumina and beta-alumina/TZ3Y samples varying %wt.

Sintering was carried out (Inti FE 1700 oven) in two stages: first at 1600°C for 20 minutes, followed by a folerived by a fast cooling up to 1475°C, soaking time of 2 hours. Use the sample is maintaned at 1600°C the temperature rises for a long time, there is an abnormal growth of grains and excessive loss of sodium, making it necessary to apply a heat treatment at a lower temperature so that a complete conversion in β phase occurs.

CHARACTERIZATION

The X-ray diffractometry analyzes (Panalytical, MRD-XL), were performed in the interval of 2θ between 10° to 80°. In order to identify possible phases. The diffractograms peaks were analyzed using Oxford® Crystallographica Search-Match software.

Scanning electron microscopy (Inspect F-50, FEI, Netherlands) was used to analyze the microstructure of sintered samples. The detector used was the secondary electron detector and the acceleration voltage, 10 kV.

Subsequently, the samples were characterized at the national nanotechnology laboratory at the energy and materials research center in Campinas-SP, Brazil (LNNano-CNPEM) by Kelvin probe (KPFM) atomic force microscopy (Atomic Force Microscopy Park NX10) used to reveal the electrical potential distribution and the topology of the electrolyte surfaces, the images were analyzed using the Gwyddion ® software.

KPFM measurements were also performed on the flat and fracture surface of a Na-β-

alumina electrolyte and the ceramic composite Na-β-alumina/TZ3Y partially stabilized with 3% yttria to characterize the change in the distribution of electrical potential. KPFM measures the difference in contact potential (CPD) between the tip and the sample, which reflects the variation of the work function between the probe tip and the electrolyte surface, resulting in the distribution of the electrical potential of the sample surfaces.

RESULTS

Figure 2 shows X-ray diffractograms of pressureless samples sintered at 1600°C for 20min and 1475°C for 2h of Na-β-alumina (100β) and the composite Na-β-alumina/TZ3Y (70β30Z, 80β20Z and 90β10Z). The identification of sodium beta-alumina peaks was performed with the aid of the Crystallographica Search-Match program. The Na-β-alumina peaks were identified: the hexagonal structure representing the β phase (ICSD 74443) and the rhombohedral structure, the β´´ phase (ICSD 70049) respectively. From the diffraction analysis, the main peaks of β and β´´ are located in the 2θ range from 30° to 50°. The formation of a mixture of phases (β/β``) [7] was observed, as expected, for 100β samples, as well as for samples with different addition concentrations of stabilized zirconia.

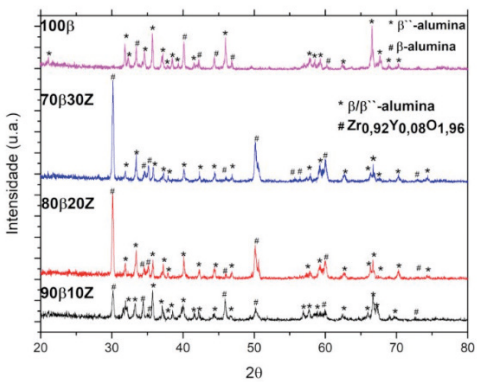

Figure 1: X-ray diffractograms of Na-β-alumina (100β) and Na-β-alumina/TZ3Y (70β30Z, 80β20Z and 90β10Z) samples sintered at 1600°C 20min and 1475°C 2h

The morphologies of fracture surfaces of sodium beta-alumina samples were observed by scanning electron microscopy, figure 2. The β/β´´-alumina phase presents a duplex microstructure, formed by a fine grain matrix, elongated grains are distributed (figure 3.a), corroborating studies performed several authors [2,3,4] who reported the formation of a duplex microstructure. The matrix consists of fine grains <10μm (figure 3.b).

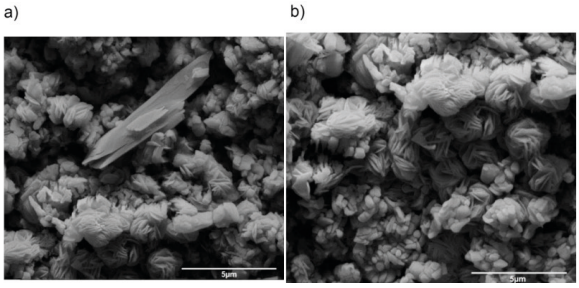

Figure 3: Micrographs of the fracture surface of Na-β-alumina sintered at 1600°C 20min followed and 1475°C 2h.

The results the show maps of contact potential between the surface and the tip of the probe and the topographic images of the electrolyte Na-β-alumina, respectively. (Figure 4). The surface was flat enough to perform the measurements of atomic force microscopy (AFM), different from the fracture surface with irregularities in its extension, we can highlight the darker regions, which are orifices derived from voids. The analyzed regions of the flat surface showed lower capacitance value (10.87 mV) when compared to the other regions, of the fracture surface (11.03 mV) and, therefore, are clearly visible, in view of the predominance of lighter color on the map of difference in contact potential on the fracture surface. The destination between regions corresponding to material and the solid electrolyte were difficult to distinguish, but presented slightly different contact potential values.

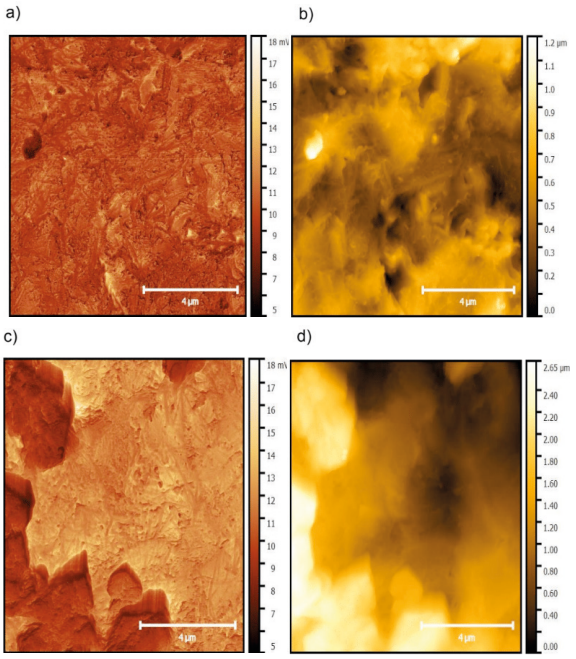

Figure 4: KPFM results of the Na-β-alumina sample (a) distribution in contact potential of the flat surface; (b) topographic image of the flat surface; (c) distribution in contact potential of the fracture surface and (d) topographic image of the fracture surface.

Figure 5 shows the images of the distribution of contact potential of the Na-β-alumina/TZ3Y, as a function of the wt% of both oxides. The regions rich stabilized zirconia with 3 mol% of yttria, exhibited, lower values of contact potential compared to other regions, exhibited by in darker images in compraisons to the images of pure Na-β-alumina. The regions of the composite material that make up the solid electrolyte were easier to distinguish, as the darker regions presenting a more insulating resulting from the presence of zirconia showied different electrical potential difference values (± 1-2 mV).

One can see that the contact potential distribution changed completely with an increase in TZ3Y(%wt), as shown in Figure 5 (a, c, e). The values of difference in contact potential in the composite electrolyte (Na-β-alumina/TZ3Y) decreased in general due to the decrease in electrical potential. In addition, the contrast between each material has changed. In contrast to Fig. 5 (e), the partially stabilized zirconia regions were lighter than other images of the material, Na-β-alumina. In addition, the contrast in contact potential between Na-β-alumina and the composite electrolyte Na-β-alumina/TZ3Y was reduced by ± 2.71 mV.

As a result, the interface between these two materials became evident. First, one may pay attention to the variation of the values of difference in contact potential in the current collector and, as the value change in this region was purely induced by the change in electrostatic potential (not by the electrochemical reaction and/or change in the work function), it is expected to correspond to the variation of the cell voltage. The analyzed regions of the surface of the solid composite electrolyte Na-β-alumina/TZ3Y, exhibited lower capacitance values as a function of the increase of zirconia added: 10% TZ3Y, 20% TZ3Y and 30% TZ3Y presented capacitance values of 10.31 mv, 9.05 mV and 8.32 mV respectively.

However, the small variation (2.71 mV: from 8.32 mV to 11.3 mV) can be explained by the so-called tip average effect included in the amplitude modulation (AM) -KPFM measurements; [1] in a previous work, the difference in contact potential (where polarization voltages were applied) with a 50 µm interval was lower than the expected value. In our case, the region of the solid electrolyte (which has lower contact potential difference values and, therefore, can decrease the contact potential difference values) is about 10 µm from the collector regions. Considering the geometric difference of the work [21.22], the influence of the average effect of the probe tip can be effectively suppressed using a frequency modulation KPFM mode [20], which allows more quantitative measurements.

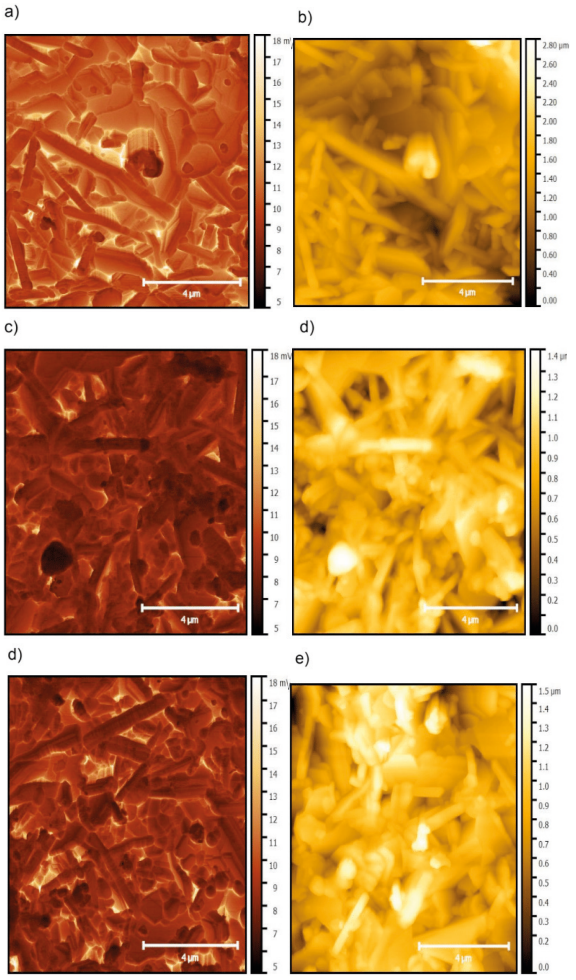

Figure 5: KPFM results of the Na-β-alumina sample with the addition of TZ3Y (a) difference in contact potential of the 90β10Z sample surface; (b) topographic image of the 90β10Z sample surface; (c) distribution in contact potential of the sample surface of 80β20Z; (d) topographic image of the surface of the 80β20Z sample; (e) distribution in contact potential of the surface of the 70β30Z sample and (f) topographic image of the 70β30Z sample.

In fact, a difference in potential gradient was observed around the interface between the composite and the β-Al_2O_3 ceramic. However, it is difficult to define a clear interface between them, which makes it impossible to discuss whether an impoverished region of these ions exists in the solid electrolytic region from these data, or not. For a detailed discussion of the weakened region with Na^+ and Y^{3+}, additional experiments are needed in a well-defined interface.

In Figure 6, SEM images, the formation of the microstructures of the Na-β-alumina/TZ3Y composite is observed. The regions of the composite material present in the solid electrolyte were different, grains in the form of platelets characterize the β-alumina phase whereas the smaller grains with more spherical shapes characterize the zirconia phase, the composites presented slightly different contact potential difference values. The greater the weight ratio of the β-alumina phase, we can highlight the greater presence of elongated grains (platelets).

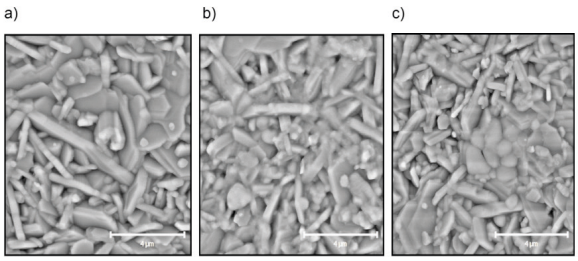

Figure 6: SEM images of the Na-β-alumina/TZ3Y sample (a) 90β10Z; (b) 80β20Z; (c)70β30Z.

The KPFM experiment also indicated that the probe has spread over the range of micrometers in the surface region of the solid electrolytes. The regions of the Na-β-Al_2O_3 ceramic surfaces and the Na-β-Al_2O_3/TZ3Y composite where the AFM/KPFM tests were carried out to obtain the results of the electrical potential presented topology values in the range of 1-1.2 μm and 1.4-2.8 μm, respectively (Figure 6). Analyzing the AFM images in Figure 4, we can highlight the sample surfaces of the Na-β-Al_2O_3 ceramic and the Na-β-Al_2O_3/TZ3Y composite.

The topography is shown in Figure 7. From these AFM images, it is clear that no major topographic changes occur on the sample surfaces of both the ceramic and the composite, in view of the possible formation

of a small layer of sodium that emerges from the formation microstructure.

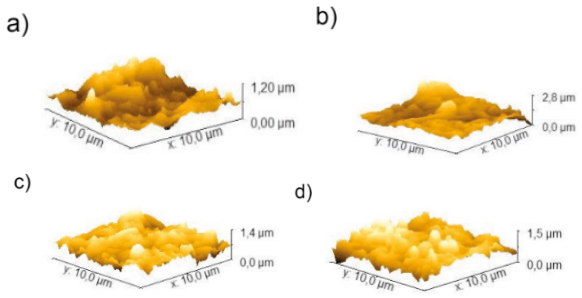

Figure 7: AFM images of the 3D topology of the Na-β-alumina and Na-β-alumina/TZ3Y sample: (a) 100β; (b) 90β10Z; (c) 80β20Z; (d) 70β30Z

In any case, some experimental results may be insufficient to conclude the general trend in the length of regions of the surface with the probe tip. Systematic experimentation on a series of different samples of the respective electrolytes, especially on well-defined interfaces, is necessary for a more detailed discussion.

This measure demonstrated that KPFM can be used to generate images of the potential distribution and topology in the solid electrolytes up to the nanoscale and to obtain information about the transport of the Na^+ and Y^{3+} ions correlated with the structure in the electrodes. Thus, the method would be important in the characterization of solid electrolytes in many aspects, such as visualizing the conductivity network in compound electrodes and clarifying the degradation mechanisms of the battery's performance. In addition, by extending our technique to measurements under operating conditions (during loading / unloading processes), it would be possible to visualize and quantify the internal resistance of cells of this type.

CONCLUSIONS

The formation of a mixture of phases (β/β``) was observed, as expected, for samples of 100β, as well as for samples with different concentrations of stabilized zirconia addition. The β/β´´-alumina phase presented a duplex microstructure, formed by a matrix of fine grains. The regions of the composite material present in the solid electrolyte were different, the platelet-shaped grains characterize the β-alumina phase while the grains smaller with more spherical shapes characterize the zirconia phase, the composites presented slightly different contact potential difference values. The greater the weight ratio of the β-alumina phase, we can highlight the greater presence of elongated grains (platelets).

The distribution of the contact potential of Na-β-alumina/TZ3Y, as a function of % by weight of both oxides, showed that the regions rich in zirconia stabilized with 3 mol% of yttria, exhibited lower contact potential values in comparison with other regions. The regions of the composite material that make up the solid electrolyte were easier to distinguish, as the darker and more insulating regions resulting from the presence of zirconia had different values of electrical potential difference (± 1-2 mV). The analyzed regions of the surface of the Na-β-alumina/TZ3Y solid composite electrolyte exhibited lower capacitance values as a function of the increase in added zirconia: 10% TZ3Y, 20% TZ3Y and 30% TZ3Y presented capacitance values of 10.31 mv , 9.05 mV and 8.32 mV, respectively.

The regions of the ceramic surfaces of Na-β-Al_2O_3 and the composite Na-β-Al_2O_3 / TZ3Y where the AFM/KPFM tests were performed to obtain the electrical potential results presented topology values in the range of 1-1.2 µm and 1.4-2.8 µm.

ACKNOWLEDGMENTS

The authors thank the Brazilian federal government agency CAPES (process 88882.180191/2018-01), the support offered by Carlos Costa the national nanotechnology laboratory at the energy and materials research center in Campinas-SP, Brazil (LNNano-CNPEM).

REFERENCES

1- D.H. Doughty, P.C. Butler, A.A. Akhil, N.H. Clark, J.D. Boyes, Batteries for large-scale Stationary electrical energy storage, Journal Eletrochem. Soc. Interface 19 (2010) 49, doi:http://dx.doi.org/10.1149/2.F05103if

2- Z. Yang, J. Zhang, M.C.W. Kintner-Meyer, D. Choi, J.P. Lemmon, J. Liu, Electrochemical energy storage for green grid, Chem. Ver. 111 (5) (2011)3 3577, doi:http://dx.doi.org/10.1021/cr100290v.

3- D.H. Lee, S.S. Han, Y.H. Kim, S.K. Lim, Analysis of crystal phases of Na^{+}-β/β´´-alumina/YSZ composite prepared by vapor-phase synthesis from YSZ-toughened α-alumina, J. Indust. And eng. Chem. (2019), doi:http://doi.org/10.1016/j.jiec_2019.04.002.

4- Yung-Fang Yu Yao, J.T. Kummer, J. Inorg. Nucl. Chem. 29 (9) (1967) 2453, doi:http://dx.doi.org/10.1016/0022-1902(67)80301-4.

5- J. Certo, C.S. Furtado, A.J. Ferreira, J.M. Perdigão, Ionics 4 (1998)124, doi:http://dx.doi.org/10.1007/BFO2375790.

6- J. Fally, C. Lasne, Y. Lazennec, P. Margotin, J. Eletrochem. Soc 120 (10)(1973)1292, doi:http://dx.doi.org/10.1149/1.2403249.

7- X. Lu, G. Xia, J.P. Lemmon, Z. Yang, Advanced materials for sodium-beta alumina batteries: Status, challenges and perspectives. Journal Power Sources vol. 195, p.2431, 2010.

8- G.E. Youngblood, A.V. Virkar, W.R. Cannon, R.S. Gordon, Bull. Amer. Ceram. Soc. 56(2) (1977) 206.

9- A. Van Zyl, M.M. Thackeray, G.K. Duncan, A.I.Kingon, R.O. Heckroodt, Mater Res. Bull 28 (2) (1993) 145.

10- A.V. Virkar, J.F. Jue and K.Z. Fung, Alkail metal beta and beta´´alumina and gallate polycrystalline ceramics and fabrication by a vapor phase process, U.S. Pattent No.6117807, september 12,2000.

11- P. Parthasarathy, N. Weber, A.V. Virkar, ECS Trans 6 (14) (2007) 67, doi:http://dx.doi.org/10.1149/1.2811944

12- M. Han, X. Tang, H. Yin, Suping Peng J. Power Sources 165 (2) (2007) 757, doi:http://dx.doi.org/10.1016/j.jpowsour.2006.11.054.

13- M. Liu, M.E. Lynch, K. Blinn, F.M. Alamgir, Y.M. Choi, Materials Today 14 (11) (2011) 534, doi:http://dx.doi.org/10.1016/S1369-7021 (11)70279-6.

14- R. A. M. Meneses, Effect of the addition of rare earth oxides on the ionic conductivity of ceramics based on ZrO2: 3 mol Y2O3 for applications in oxygen sensors. 92 f, 2010

15- V. L. Arantes, R.B. Coutinho, S.S. Martins, S. Huang, J. Vleugels Solid Sintering Behavior of zirconia-nickel composites Ceramics International, 45 (2019) pp22120-22130 https://doi.org/10.1016/j.ceramint.2019.07.229

16- S. De Souza, S.J. Visco, L.C. De Jonghe, J. Eletrochem. Soc. 144 (3) (1997) L35, doi:http://dx.doi.org/10.1149/1.1837484.

17- A. Eichier, Physical Review B 64 (2001) 174103-1, doi:http://dx.doi.org/10.1103/PhysReB.64.174103.

18- F.F. Lange, B.J. Davis, D.O. Raleigh, J. Am. Ceram. Soc. 66 (3) (1983) C50, doi:http://dx.doi.org/10.1111/j.1151-2916.1983.tb03507.x.

19- D.J. Green, J. Mater Sci 20 (7) (1985) 2639, doi:http://dx.doi.org/10.1007/BF00556096.

20- A.V. Virkar, J. Mater Sci 16 (5) (1981) 1142, doi:http://dx.doi.org/10.101007/BF01033824.

21- D. S. H. Charrier, M. Kemerink, B. E. Smalbrugge, T. de Vries and R. A. J. Janssen, ACS Nano, 2008,2, 622-626.

22- V. Panchal, R. Pearce, R. Yakimova, A. Tzalenchuk and O. Kazakova, Science Rep., 2013, 3, 2597.

23- S. Campanari, L. Mastropasqua, M. Gazzani, P. Chiesa, M.C. Romano Predicting the ultimate potential of natural gas SOFC power cycles with CO_2 capture - Part B: Applications J. Power Sources., 325 (2016), pp. 194-208, https://doi.org/10.1016/j.jpowsour.2016.05.134

24- J. Gao, Q. Li, W. Xia, L. Sun, L.H. Huo, H. Zhao Advanced electrochemical performance and CO_2 tolerance of $Bi_{0.5}Sr_{0.5}Fe_{1-x}Ti_xO_{3-\delta}$ perovskite materials as oxygen reduction cathodes for intermediate-temperature solid oxide fuel cells ACS Sustain Chem. Eng., 7 (2019), pp. 18647-18656, https://doi.org/10.1021/acssuschemeng.9b05086

25- A. Pandiyan, V. Di Palma, V. Kyriakou, W.M.M. Kessels, M. Creatore, M.C.M. Van De Sanden, M.N. Tsampas Enhancing the electrocatalytic activity of redox stable perovskite fuel electrodes in solid oxide cells by atomic layer-deposited pt nanoparticles ACS Sustain. Chem. Eng., 8 (2020), pp. 12646-12654, https://doi.org/10.1021/acssuschemeng.0c04274

26- L. Xing, T. Xia, Q. Li, H. Zhao, L. Sun, L.H. Huo High-performance and CO_2-durable composite cathodes toward electrocatalytic oxygen reduction: Ce0.8Sm0.2O1.9 nanoparticle-decorated double perovskite $EuBa_{0.5}Sr_{0.5}Co_2O_{5+\delta}$ ACS Sustain Chem. Eng., 7 (2019), pp. 17907-17918, https://doi.org/10.1021/acssuschemeng.9b04533

27- S. Hu, W. Li, W. Li, N. Zhang, H. Qi, H. Finklea, X. Liu A study on the electrophoretic deposition of gadolinium doped ceria on polypyrrole coated yttrium stabilized zirconia J. Colloid Interface Sci., 555 (2019), pp. 115-123, https://doi.org/10.1016/j.jcis.2019.07.094

28- F.S. da Silva, T.M. de Souza Novel materials for solid oxide fuel cell technologies: A literature review Int. J. Hydrogen Energy., 42 (2017), pp. 26020-26036, https://doi.org/10.1016/j.ijhydene.2017.08.105

29- T.L. Simonenko, M.V. Kalinina, N.P. Simonenko, E.P. Simonenko, O.V. Glumov, N.A. Mel'nikova, I.V. Murin, O.O. Shichalin, E.K. Papynov, O.A. Shilova, V.G. Sevastyanov, N.T. Kuznetsov Synthesis of $BaCe_{0.9-x}Zr_xY_{0.1}O_{3-\delta}$ nanopowders and the study of proton conductors fabricated on their basis by low-temperature spark plasma sintering Int. J. Hydrogen Energy., 44 (2019), pp. 20345-20354, https://doi.org/10.1016/j.ijhydene.2019.05.231

30- L.S. Mahmud, A. Muchtar, M.R. Somalu Challenges in fabricating planar solid oxide fuel cells: A review Renew. Sustain. Energy Rev., 72 (2017), pp. 105-116, https://doi.org/10.1016/j.rser.2017.01.019